



# Sid2 regulates hepatocellular lipid metabolism through autophagy

Xueru Chen, Xuefan Gu,<sup>1</sup> and Huiwen Zhang<sup>1</sup>

Department of Pediatric Endocrinology and Genetic Metabolism, Xinhua Hospital, Shanghai Institute for Pediatric Research, Shanghai Jiao Tong University School of Medicine, Shanghai, China

**Abstract** SID1 transmembrane family member 2 (*Sid2*) is an integral lysosomal membrane protein. To investigate its explicit function, we generated a global *Sid2* knockout mouse model (*Sid2*<sup>-/-</sup>). Compared with the littermate controls, *Sid2*<sup>-/-</sup> mice exhibited a remarkable accumulation of lipid droplets in liver. First, it was observed that food consumption, hepatocyte fatty acid uptake and de novo lipogenesis, hepatocyte lipolysis, and TG secretion in the form of very low density lipoprotein were comparable between *Sid2*<sup>-/-</sup> and WT mice. However, the hepatic  $\beta$ -oxidation of fatty acids decreased significantly as revealed by a low level of serum  $\beta$ -hydroxybutyrate in the *Sid2*<sup>-/-</sup> mice along with normal mRNA expression of genes involved in fatty acid oxidation. In addition, the classical autophagy pathway marker proteins, p62 and LC3-II, increased in liver, along with compromised autophagic flux in primary hepatocytes, indicating a block of autophagosome maturation due to *Sid2* deficiency, which was also supported by electron microscopy image analysis both in livers and in primary hepatocytes from *Sid2*<sup>-/-</sup> mice. It was concluded that *Sid2* plays an important role in mouse hepatic lipid homeostasis by regulating autophagy at the terminal stage.—Chen, X., X. Gu, and H. Zhang. *Sid2* regulates hepatocellular lipid metabolism through autophagy. *J. Lipid Res.* 2018. 59: 404–415.

**Supplementary key words** SID1 transmembrane family member 2 • lipid droplets • triglycerides • liver metabolism

Lysosomes and lysosome-related organelles form a highly efficient and coordinated metabolic regulatory network. The functions of this system include various physiological processes, such as cholesterol homeostasis (1), pathogen defense (2), plasma membrane repair (3), and bone and tissue remodeling (4). However, its major task is the degradation of extracellular material and intracellular components taken up by endocytosis and autophagy (1). The degraded products, which may include amino acids, sugars, simple glycolipids, cholesterol, and nucleotides, are

salvaged and delivered to other cellular organelles and membranes for reutilization. The proper function of lysosomes is essential for cellular metabolic homeostasis; dysfunction can result in around 50 different types of lysosomal storage disorders (5). In addition, increasing evidence reveals that lysosomes are involved in more widespread diseases, such as cancer, Alzheimer's disease, cardiovascular diseases, and nonalcoholic fatty liver disease (NAFLD) (6–9).

Excess fat accumulation in the liver can occur as a result of enhanced fatty acid delivery, increased de novo lipogenesis, reduced lipolysis and fat export in the form of very low density lipoproteins, and decreased fatty acid oxidation (10, 11). Recent evidence has shown that the lysosomal-autophagic pathway plays an important part in hepatocyte lipid metabolism, and that defective autophagy may contribute to the pathogenesis of NAFLD by decreasing fatty acid oxidation (12). However, the factors that connect autophagy with lipid metabolism urgently await discovery.

Lysosomal membrane proteins (LMPs) are vital for lysosomes' executive function. They play diverse roles, including acidification of the lysosomal lumen, fusion of the cellular membrane system, and transportation of degradation products (13, 14). Approximately 58 LMPs have been identified (15). Of these, lysosome-associated membrane protein (LAMP)-1, LAMP-2, lysosomal integral membrane protein (LIMP)-2, and CD63 are the most abundant (16). However, more potential LMPs continue to be revealed by proteomics analysis with their exact physical function to be explored (17, 18).

SID1 transmembrane family member 2 (*Sid2*) is an integral LMP that is widely expressed in all tissues (19). Previously, to understand the function of *Sid2* in vivo, we

Abbreviations: ADFP, adipocyte differentiation-related protein; ASMase, acid sphingomyelinase; Cpt, carnitine palmitoyltransferase; Dgat, diacylglycerol O-acyltransferase; EM, electron microscopy; HF, high-fat; Hsl, hormone sensitive lipase; LAMP, lysosome-associated membrane protein; LD, lipid droplet; LMP, lysosomal membrane protein; NAFLD, nonalcoholic fatty liver disease; OA, oleic acid; RM, regular medium; *Sid2*, SID1 transmembrane family member 2; TBST, TBS with 0.1% Tween 20; TFEB, transcription factor EB; TG, triglyceride.

<sup>1</sup>To whom correspondence should be addressed.

e-mail: gu\_xuefan@163.com (X.G.); huiwenzhang@yahoo.com (H.Z.)

This work was supported by National Natural Science Foundation of China Grants 81570516 and 81270936, Shanghai Science and Technology Committee Grant 16JC1404600, and Shanghai Municipal Education Commission Grant 20152520 (to H.Z.).

Manuscript received 1 December 2016 and in revised form 23 January 2018.

Published, JLR Papers in Press, January 23, 2018

DOI <https://doi.org/10.1194/jlr.M073817>

generated a global *Sid2* gene knockout mouse model and observed impaired glucose tolerance likely due to compromised NAADP-involved insulin secretion (20). Here, we demonstrated that *Sid2* also plays an important role in hepatocyte lipid metabolism by regulating hepatic lipid autophagy.

## MATERIALS AND METHODS

### Animals

*Sid2*<sup>-/-</sup> mice were generated as previously described (21). All mice were housed with standard temperature and humidity and were maintained on a 12 h light/dark cycle. Mice were fed a standard chow diet or a high-fat (HF) diet (60% kcal in fat; Research Diets, D12492) and had free access to water. The HF diet began at 6 weeks of age and continued for a total of 12 weeks. In all studies, gender- and age-matched homozygous knockout animals were compared with WT controls, which were littermates of the knockout mice. Male mice at 14 weeks of age were used in our study. In selected experiments, 6-week-old male mice were used. All experiments involving mice were approved by Institutional Review Ethics Board of Xinhua Hospital.

### Primary hepatocyte isolation and culture

Mouse primary hepatocytes were isolated from 10-week-old male *Sid2*<sup>-/-</sup> and WT mice by two-step perfusion, as previously described (22). The liver was perfused with Hanks' balanced salt solution (Gibco) containing 1 mM EDTA, and then digested with Hanks' balanced salt solution (Gibco) containing 0.05% collagenase IV (Sigma). The dissociated cells were then filtered through a 100 μm cell strainer and centrifuged at 35 *g* for 5 min at 4°C. Hepatocytes were washed twice with PBS, followed by centrifugation at 500 rpm for 5 min at 4°C, and then resuspended and seeded in a 6-well plate at a concentration of 3 × 10<sup>5</sup> cells/well in hepatocyte medium (ScienCell 5201; 5% fetal bovine serum, 1% penicillin/streptomycin solution, and 1% hepatocyte growth supplement). After 24 h, hepatocytes were maintained in DMEM (Gibco) containing 10% fetal bovine serum, 1% penicillin/streptomycin solution, and 1% L-glutamine.

### Oil Red O staining

Oleic acid (OA; Sigma-Aldrich) was conjugated to fatty acid-free BSA, as described previously (23). In brief, 20 mM of OA in 0.1 mol/l NaOH were incubated at 70°C for 30 min and fatty acid soaps were then complexed with 20% BSA at a 6:1 molar ratio of fatty acid to BSA. Primary hepatocytes were treated with 0.2 mM of OA for 24 h in DMEM with 1% fetal bovine serum, and were subsequently fixed in 3.7% formaldehyde for 15 min and stained with Oil Red O (Sigma-Aldrich) in 60% isopropanol for 20 min. After washing with 60% isopropanol for 30 s, the cells were redyed with hematoxylin for 4 min. Lipid droplets (LDs) stained in red were assessed by bright-field microscopy and quantified using the ImageJ software (The National Institutes of Health).

### Western blotting

Cells were washed twice with cold PBS before being lysed on ice in RIPA buffer with PMSF (Sigma-Aldrich). Liver tissue samples (30 mg) were submerged in RIPA buffer supplemented with PMSF, leupeptin, and pepstatin inhibitors, and then minced with scissors and homogenized with a MagNA Lysor (Roche Applied Science) for 1 min. Homogenates were centrifuged at 13,800 *g* for 20 min at 4°C. Supernatants were collected and quantified for protein concentration using a BCA kit (Bio-Rad).

Proteins were resolved on SDS-PAGE and then transferred onto polyvinylidene difluoride membranes (Millipore). Membranes were blocked in TBS with 0.1% Tween 20 (TBST) containing 5% nonfat dry milk and incubated with primary antibodies overnight at 4°C. The primary antibodies used in the present study included rabbit anti-LC3B (1:1,000; Sigma-Aldrich), rabbit anti-p62/SQSTM1 (1:1,000; Cell Signaling Technology), rabbit anti-ADRP (1:1,000; Novus Biologicals), rabbit anti-Atg5 (1:1,000; Cell Signaling Technology), rabbit anti-Atg7 (1:1,000; Cell Signaling Technology), rabbit anti-beclin-1 (1:1,000; Cell Signaling Technology), rabbit anti-transcription factor EB (TFEB) (1:1,000; Santa Cruz Biotechnology), rabbit anti-phospho-4E-BP1 (1:1,000; Cell Signaling Technology), rabbit anti-4E-BP1 (1:1,000; Cell Signaling Technology), rabbit anti-phospho-p70 S6 kinase (1:1,000; Cell Signaling Technology), rabbit anti-p70S6 kinase (1:1,000; Cell Signaling Technology), rat anti-Lamp2 (1:1,000; Developmental Studies Hybridoma Bank), mouse anti-cathepsin B (1:400; Abcam), mouse anti-cathepsin D (1:1,000; Abcam), mouse anti-β-actin (1:5,000; Beyotime), mouse anti-tubulin (1:1,000; Beyotime), and mouse anti-GAPDH (1:5,000; KangChen). Membranes were washed three times in TBST and incubated with the corresponding HRP-conjugated secondary antibody (1:5,000; Santa Cruz Biotechnology) at room temperature for 1 h. Finally, blots were washed three times with TBST and bands were detected using an enhanced chemiluminescence system (Thermo Scientific).

### Histological studies

Liver tissue was taken from age- and sex-matched mice. Tissues were fixed in 4% formalin and paraffin-embedded, and then sections were stained with hematoxylin/eosin. The segments of liver were embedded in optimal cutting temperature compound (Sakura) and cryostat-sectioned at a thickness of 5 μm for lipid deposition assessment via Oil Red O staining. Quantification of hepatocytes' size and Oil Red O-stained area was performed by the ImageJ software after appropriate thresholding.

### Electron microscopy

Cells cultured in monolayers and liver blocks (1 mm<sup>3</sup> in size) were fixed in 2% glutaraldehyde in PBS (pH 7.2) for 2 h, and then postfixed in 1% osmium tetroxide for 2 h. Samples were then dehydrated with an ascending series of alcohol before embedding in Araldite. Ultra-thin sections were cut and stained with lead citrate. Images were acquired with an electron microscope (CM-120; Philips).

### Microarray analysis of liver tissue

Microarray analysis was performed in the liver as previously described (24). Extracted RNA was labeled with biotin and hybridized to Affymetrix GeneChip mouse genome 430 2.0 single arrays. The hybridization was performed according to the manufacturer's instructions. Bioinformatics analysis was performed by Gene Tech, Shanghai, China. Microarray analyses of liver tissue were conducted in *Sid2*<sup>-/-</sup> and WT mice at 1, 3, and 6 months of age, respectively. The raw CEL files were background corrected on the perfect match values and normalized by the Robust Multichip Array algorithm. Principal component analysis was performed and one-way ANOVA was performed to identify differentially expressed genes (fold-change >2) among groups.

### Quantitative real-time PCR

Total RNA was isolated from liver tissue using Trizol (Invitrogen) and cDNA was synthesized from 500 ng RNA by the PrimeScript™ RT reagent kit (Takara), according to the manufacturer's instructions. Real-time PCR was performed on a 7500/7500 FAST real-time PCR system (Applied Biosystems) using a SYBR® Premix

Ex Taq™ kit (Takara). Actin levels were measured for normalization. Primer sequences are available on request.

### Assay of serum NEFA

Mice were fasted overnight and blood was isolated by retro-orbital bleeding. Serum NEFA was measured with a commercially available kit (Wako), according to the manufacturer's instructions.

### Assay of hepatic triglyceride secretion

Triglyceride (TG) secretion was determined as described previously (25). Mice were fasted for 6 h and then injected intraperitoneally with 1 g/kg of poloxamer-407 (Sigma-Aldrich). Plasma samples were drawn prior to and after injection for TG measurements. The TG production rate was calculated based on serum TG level changes and expressed as micromoles per kilogram per hour.

### Analysis of liver lipids

Mice were fasted overnight and liver TG was determined as described previously (26). Briefly, approximately 200 mg of liver (wet weight) were digested by ethanolic KOH and incubated overnight at 55°C. On the second day, water:ethanol (1:1 v/v) was added to the tube and then the mixture was centrifuged. The supernatant was treated with water:ethanol again followed by neutralization with MgCl<sub>2</sub>. The supernatant obtained by centrifugation was ready for further analyses. Liver TG content was determined using a TG determination kit (Sigma-Aldrich).

### Measurement of serum β-hydroxybutyrate

Serum β-hydroxybutyrate levels were measured in 6 h-fasted serum samples using the β-hydroxybutyrate assay kit from Abcam.

### Determination of acid sphingomyelinase activity

Acid sphingomyelinase (ASMase) activity from liver lysates was determined using a fluorescent substrate (6-HMU-phosphorylcholine; Moscerdam). Homogenates containing 50 μg of protein from liver tissue were incubated with 10 μl of 1.35 mmol/l 6-HMU-phosphorylcholine in 0.1 mmol/l sodium acetate (pH 5.2) for 17 h at 37°C. The reaction was stopped by adding 200 μl of glycine/NaHCO<sub>3</sub> buffer with 0.25% Triton X-100 (pH 10.5). The fluorescence signal was read with a fluorometric plate reader (Perkin Elmer) using an excitation wavelength of 365 nm and an emission wavelength of 450 nm.

### Statistical analysis

All data are presented as mean ± SEM. A Student's *t*-test was used for statistical comparison and *P* ≤ 0.05 was considered significant.

## RESULTS

### LDs accumulate in the livers of *Sid2*<sup>-/-</sup> mice

The volume of livers in *Sid2*<sup>-/-</sup> mice increased. Consistent with their increased liver volume, the ratio of liver weight to total body weight also significantly increased compared with control mice (Fig. 1A). Although the *Sid2*<sup>-/-</sup> mice weighed less than the WT mice at 6 weeks of age (21), there was no significant difference in body weight between the two groups after HF diet for 12 weeks (Fig. 1B). Histological analysis of liver specimens revealed that abundant round vesicles resembling LDs accumulated in

*Sid2*<sup>-/-</sup> mice fed chow diets. Moreover, hepatocytes from *Sid2*-deficient mice had bigger cell sizes than WT mice and appeared hypertrophic, and consequently sinusoids appeared small (Fig. 1C). Neither significant inflammatory cell infiltration nor ballooning degeneration were observed, indicating no steatohepatitis at this stage (Fig. 1C). In mice fed a HF diet, the livers of the *Sid2*<sup>-/-</sup> mice not only contained many more LDs than those of WT mice, but also showed ballooning degeneration (Fig. 1C). Furthermore, the livers of *Sid2*<sup>-/-</sup> mice fed chow or HF diet contained many more Oil Red O-positive vacuoles than those of WT mice, suggesting an accumulation of LDs in the liver of *Sid2*<sup>-/-</sup> mice (Fig. 1D). Transmission electron microscopy (EM) studies further confirmed that both the number and size of the hepatic LDs were markedly increased in the livers of *Sid2*<sup>-/-</sup> mice fed a chow diet after fasting (Fig. 1E). The accumulation of LDs in *Sid2*<sup>-/-</sup> mice was also confirmed by an elevated level of the adipocyte differentiation-related protein (ADRP or ADFP), a LD-associated protein (Fig. 1G). Finally, we measured the level of TG in the livers of *Sid2*<sup>-/-</sup> mice. TG levels in the livers of *Sid2*<sup>-/-</sup> mice fed a chow diet were ~140% higher than in WT mice; and in mice with an HF diet, the proportion was more than 160% (Fig. 1H).

In addition, increased lipid staining with Oil Red O was observed in primary hepatocytes from *Sid2*<sup>-/-</sup> mice, indicative of an accumulation of LDs both under regular medium (RM) and following a supply of exogenous OA (Fig. 1F). Taken together, these results indicate that *Sid2* deficiency leads to an accumulation of LDs in the liver. Consistent with these findings, *Sid2* deficiency caused a marked elevation of serum ALT and AST in mice fed both chow and HF diets (Fig. 1I), indicating considerable hepatocellular injury by LD accumulation.

### Impact of *Sid2* knockout on major pathways of TG metabolism

To investigate the reason for TG accumulation, we first looked into food consumption in *Sid2*<sup>-/-</sup> and WT mice, which did not significantly differ between the two groups (Fig. 2A).

Next, microarray analysis was conducted to examine the mRNA levels of genes usually perceived as important in NEFA uptake to the liver. These genes include solute carrier family 27 member 2 (*Slc27a2* or *Fatp2*), solute carrier family 27 member 5 (*Slc27a5* or *Fatp5*), and *CD36*. The two fatty acid transport proteins, *Slc27a2* and *Slc27a5*, did not significantly differ (Table 1), which was further demonstrated by quantitative RT-PCR performed in liver tissues of 14-week-old WT or *Sid2*<sup>-/-</sup> mice (Fig. 2B). However, *CD36* was consistently increased approximately 4-fold in *Sid2*<sup>-/-</sup> mice at 3 and 6 months of age (Table 1). Because *CD36*-null mice exhibit reduced muscle TG and liver steatosis (27), *CD36* may play a limited role in hepatocyte uptake of fatty acids. Instead, fatty acid transport proteins play a predominant role in this cellular process (10). Thus, fatty acid uptake was not significantly increased in *Sid2*<sup>-/-</sup> mice.

Data of microarray and quantitative RT-PCR also showed that most of the genes involved in de novo lipogenesis,



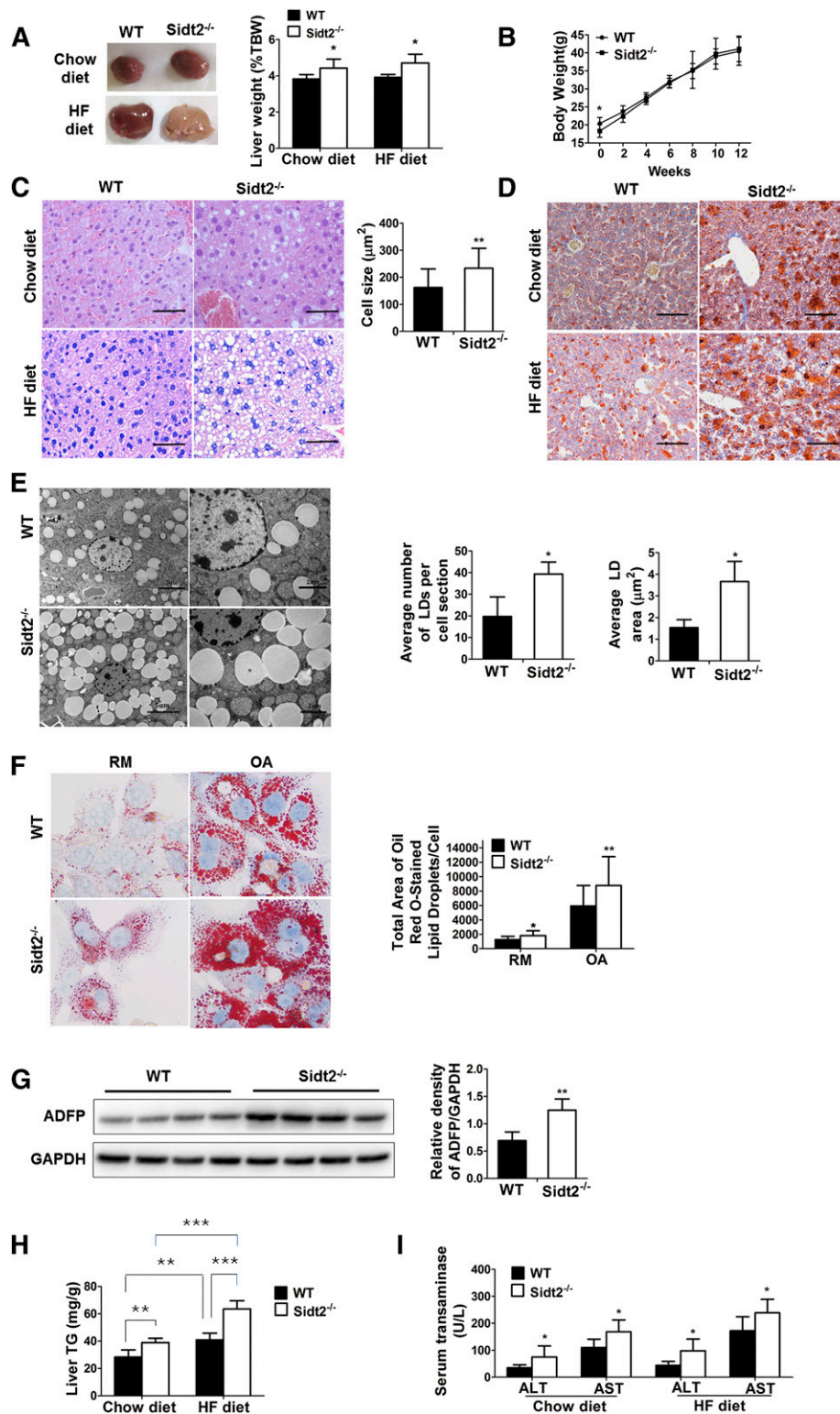


**Fig. 1.** *Sid2* knockout causes lipid accumulation in the liver. **A:** Gross view and weights of livers in chow and HF diet groups ( $n = 5$ ). **B:** Body weights of WT and *Sid2*<sup>-/-</sup> mice maintained on a HF diet for 12 weeks. **C:** H&E staining of liver from mice fed with chow diet (scale bar, 50  $\mu\text{m}$ ). The graph shows the quantification of hepatocyte size in more than 100 cells from three different mice in each group. **D:** Oil Red O staining (scale bar, 100  $\mu\text{m}$ ). **E:** Electron micrographs of liver from chow diet-fed mice without intake of food for 20 h. Scale bars, 5  $\mu\text{m}$  (left) and 2  $\mu\text{m}$  (right). The graphs show quantifications of LD number and size ( $n = 3$ ). **F:** Oil Red O staining of primary hepatocytes from *Sid2*<sup>-/-</sup> and WT mice treated with 0.2 mM OA for 24 h. Microscopic images (left, 400 $\times$ ) and quantification of Oil Red O-stained area (right) ( $n = 46$ –54 cells from three independent experiments). **G:** Immunoblot analysis of ADFP levels in livers from mice fed with chow diet ( $n = 4$ ). **H:** Hepatic TG concentration of mice fed chow or HF diets ( $n = 6$ ). **I:** Serum transaminase levels in livers from mice fed with chow diet ( $n = 6$ ). \* $P < 0.05$ , \*\* $P < 0.01$ , and \*\*\* $P < 0.001$ . TBW, total body weight.

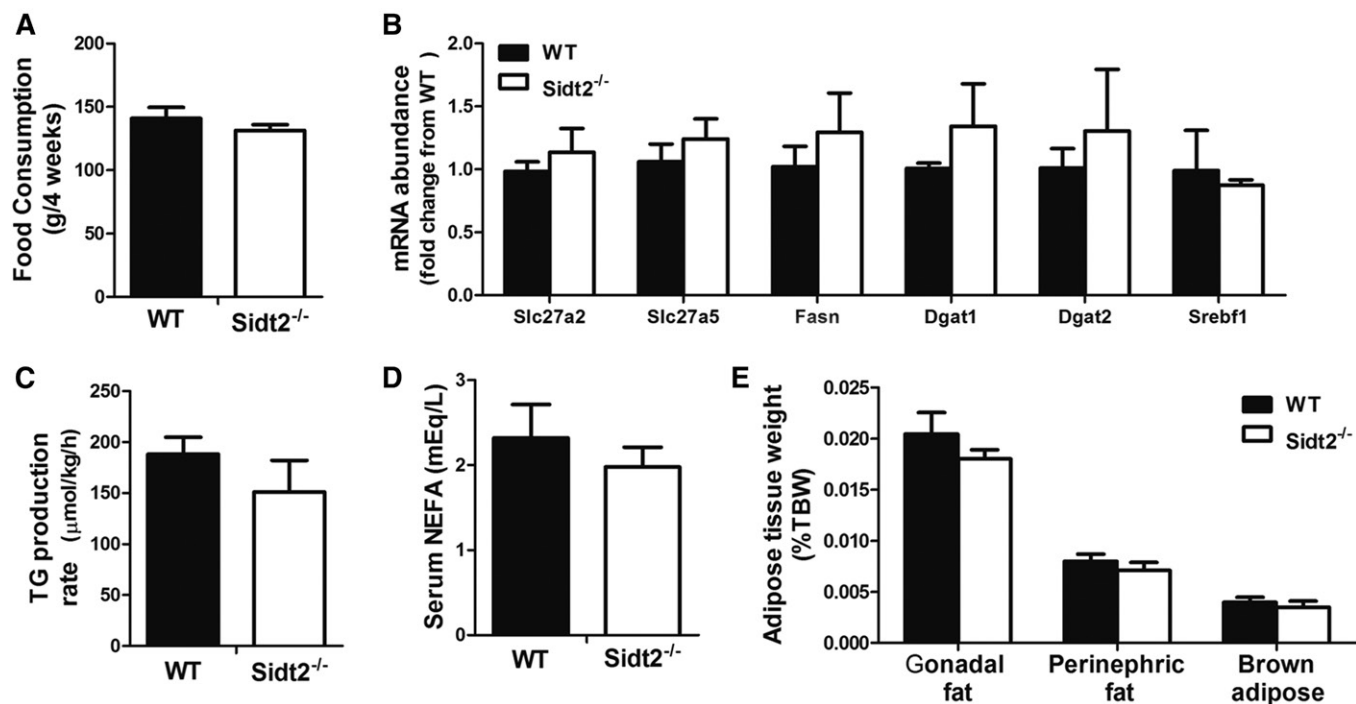


**Fig. 2.** *Sidt2* knockout does not influence lipogenesis and TG secretion. A: Total food consumption of WT or *Sidt2*<sup>-/-</sup> mice under a chow diet measured for 4 weeks beginning at 8 weeks of age (n = 8). B: Quantitative real-time PCR analysis of genes involved in lipid transport and lipogenesis in the livers of 14-week-old WT or *Sidt2*<sup>-/-</sup> mice fed a chow diet (n = 3). C: Hepatic TG production rate (n = 6). D: Serum NEFA level (n = 6). E: The weight of adipose tissues from WT or *Sidt2*<sup>-/-</sup> mice under a chow diet (n = 6). TBW, total body weight.

including *Fasn*, diacylglycerol O-acyltransferase (*Dgat1*), and *Dgat2* were not significantly changed in *Sidt2*<sup>-/-</sup> mice (Table 1, Fig. 2B). Furthermore, the master gene that

controls the expression of lipogenic genes, sterol regulatory element-binding transcription factor 1 (*Srebf1*), was not changed (Table 1, Fig. 2B). Because lipogenesis is

TABLE 1. The mRNA expression of genes involved in lipid metabolism in *Sidt2*<sup>-/-</sup> relative to WT mice

Gene Symbol	Gene Title	Fold Change (KO/WT)		
		1 Month	3 Months	6 Months
<b>Fatty acid uptake and transport</b>				
<i>Slc27a2</i>	Solute carrier family 27 member 2	1.06	1.05	-1.52
<i>Slc27a5</i>	Solute carrier family 27 member 5	-1.04	-1.16	-1.32
<i>Cd36</i>	CD36 antigen	2.04	4.73	3.64
<i>Acs11</i>	Acyl-CoA synthetase long-chain family member 1	1.20	-1.50	-2.70
<i>Fabp1</i>	Fatty acid binding protein 1	-1.02	1.07	-1.68
<b>Lipogenesis</b>				
<i>Srebf1</i>	Sterol regulatory element-binding transcription factor 1	-1.82	1.29	-1.18
<i>Acaca</i>	Acetyl-CoA carboxylase $\alpha$	-1.13	-1.09	1.02
<i>Fasn</i>	Fatty acid synthase	-1.04	-1.14	-1.25
<i>Elovl6</i>	ELOVL family member 6, elongation of long chain fatty acids	1.50	1.04	-1.03
<i>Scd1</i>	Stearoyl-CoA desaturase 1	-1.46	-1.11	1.37
<i>Acpat1</i>	1-Acylglycerol-3-phosphate O-acyltransferase 1	-1.01	-1.18	1.03
<i>Lpin1</i>	Lipin 1	2.84	-1.88	-1.02
<i>Dgat1</i>	Diacylglycerol O-acyltransferase 1	1.04	-1.06	-1.12
<i>Dgat2</i>	Diacylglycerol O-acyltransferase 2	-1.19	-1.00	-1.18
<b>Lipolysis</b>				
<i>Hsl</i>	Lipase, hormone sensitive	-1.10	-1.31	1.01
<i>Atgl</i>	Adipose TG lipase	-1.05	-1.30	-1.22
<i>Lipc</i>	Lipase, hepatic	-1.18	1.47	-2.02
<b>Fatty acid oxidation</b>				
<i>Cpt1a</i>	Carnitine palmitoyltransferase 1a, liver	-1.18	-1.11	-1.57
<i>Cpt2</i>	Carnitine palmitoyltransferase 2	1.58	1.03	-1.52
<i>Cact</i>	Mitochondrial carnitine/acylcarnitine translocase	1.37	-1.07	-1.24
<i>Ppara</i>	Peroxisome proliferator activated receptor $\alpha$	1.05	1.03	-1.85
<b>Lipoprotein assembly</b>				
<i>Mttp</i>	Microsomal TG transfer protein	1.27	1.43	-1.28

mainly controlled at the transcriptional level (28), it was concluded that de novo lipogenesis was not affected in *Sidt2*<sup>-/-</sup> mice.

Liver secretes TG in the form of very low density lipoprotein to the peripheral blood. We injected fasted mice with poloxamer-407, an inhibitor of lipoprotein lipase. Though the TG production rate was decreased by 20% in *Sidt2*<sup>-/-</sup> mice compared with WT mice, there was no significant difference between the two groups (Fig. 2C).

Simultaneously, the level of serum NEFA, the product of lipolysis in adipose tissue, was not significantly different between *Sidt2*<sup>-/-</sup> and WT mice (Fig. 2D). Consistent with the unchanged serum NEFA, the weights of adipose tissues, including gonadal fat, perinephric fat, and brown adipose, were comparable between *Sidt2*<sup>-/-</sup> and WT mice (Fig. 2E), suggesting that *Sidt2* deficiency does not induce excessive lipolysis in adipose tissue.

### *Sidt2* knockout reduces hepatic $\beta$ -oxidation of fatty acids

Fatty acid  $\beta$ -oxidation is another method of TG disposal. We measured the level of serum  $\beta$ -hydroxybutyrate, the product of hepatic fatty acid  $\beta$ -oxidation. In *Sidt2*<sup>-/-</sup> mice, serum  $\beta$ -hydroxybutyrate concentrations decreased to 68% compared with WT mice (Fig. 3A), suggesting that hepatic  $\beta$ -oxidation is impaired in *Sidt2*<sup>-/-</sup> mice.

However, the RNA microarray and the quantitative RT-PCR analyses showed the expression of genes involved in hepatic mitochondrial fatty acid oxidation, such as carnitine palmitoyltransferase (*Cpt1*), *Cpt2*, and *Ppara*, were not significantly different between *Sidt2*<sup>-/-</sup> and WT mice (Table 1, Fig. 3B). These data suggest that *Sidt2* deficiency reduced hepatic mitochondrial  $\beta$ -oxidation of fatty acids without affecting transcription of related enzymes. With the genes providing free fatty acids for mitochondrial  $\beta$ -oxidation unchanged, such as hepatic lipase (*Lipc*) and hormone sensitive lipase (*Hsl*) (Table 1, Fig. 3B), we speculated that lipophagy (12), which provides fatty acids to mitochondria, was affected in *Sidt2*<sup>-/-</sup> mice.

### Lipid metabolism impaired in 6-week-old mice

To determine when *Sidt2* began to damage hepatic lipid metabolism in mice, we evaluated lipid metabolism in 6-week-old mice. In 6-week-old *Sidt2*<sup>-/-</sup> mice, liver TG con-

tent and liver ADFP protein expression were increased, and serum  $\beta$ -hydroxybutyrate levels were decreased compared with age-matched WT mice (Fig. 4A–C). These findings confirmed that *Sidt2* deficiency led to lipid accumulation by impairing  $\beta$ -oxidation in the liver. Consistent with 14-week-old mice, no significant difference was found in serum NEFA between 6-week-old *Sidt2*<sup>-/-</sup> and WT mice (Fig. 4D).

### *Sidt2* knockout blocks hepatic autophagy in vivo

To explore whether *Sidt2* regulates liver steatosis via autophagy, we tested liver responses in *Sidt2*<sup>-/-</sup> mice. LC3-II is present in autophagosomes and is a commonly used marker of autophagy activation (29). We found that LC3-II levels were significantly elevated in the livers from *Sidt2*<sup>-/-</sup> mice fed a chow diet, compared with aged-matched WT mice, suggesting normal or increased autophagosome formation (Fig. 5A, B). In addition, p62/SQSTM1, which functions in guidance of polyubiquitinated protein to autophagosomes and sequential degradation via the autophagy pathway (27, 30), also accumulated in the livers of *Sidt2*<sup>-/-</sup> mice (Fig. 5A, C). An increase of both LC3-II and p62 levels were also observed in *Sidt2*<sup>-/-</sup> mice with HF diet (Fig. 5D–F), suggesting a defect in the autophagy pathway after autophagosome formation.

EM evaluation showed abundant autophagic vacuoles at different stages of autophagy in *Sidt2*<sup>-/-</sup> (Fig. 5H–K) compared with WT mice in vivo (Fig. 5G). *Sidt2*<sup>-/-</sup> livers had more double/multi-lamellar membrane structures containing cytosol, LDs, or other organelles (Fig. 5H). We also identified autolysosomes, vacuoles surrounded by one limiting membrane enclosing cytoplasmic material and/or organelles, at various stages of degradation (Fig. 5I, J). Therefore, EM examination supported that *Sidt2* deficiency impairs maturation of autophagosomes to autolysosomes.

### *Sidt2* knockout blocks autophagy in vitro

To further assess the role of *Sidt2* in autophagy, we analyzed autophagosome formation in primary hepatocytes isolated from *Sidt2*<sup>-/-</sup> and WT mice. Consistent with our observations in vivo, LC3-II and p62 expression in *Sidt2*<sup>-/-</sup> hepatocytes increased in the normal medium (Fig. 6A, B).

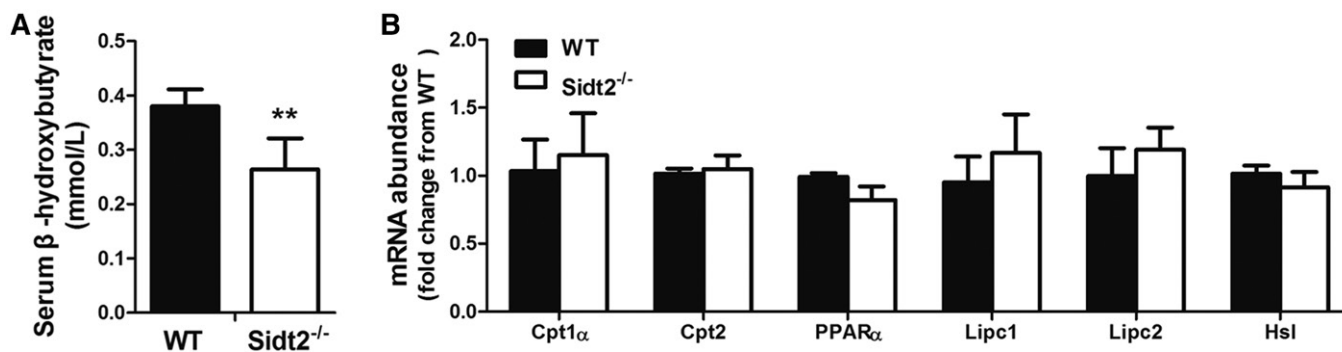
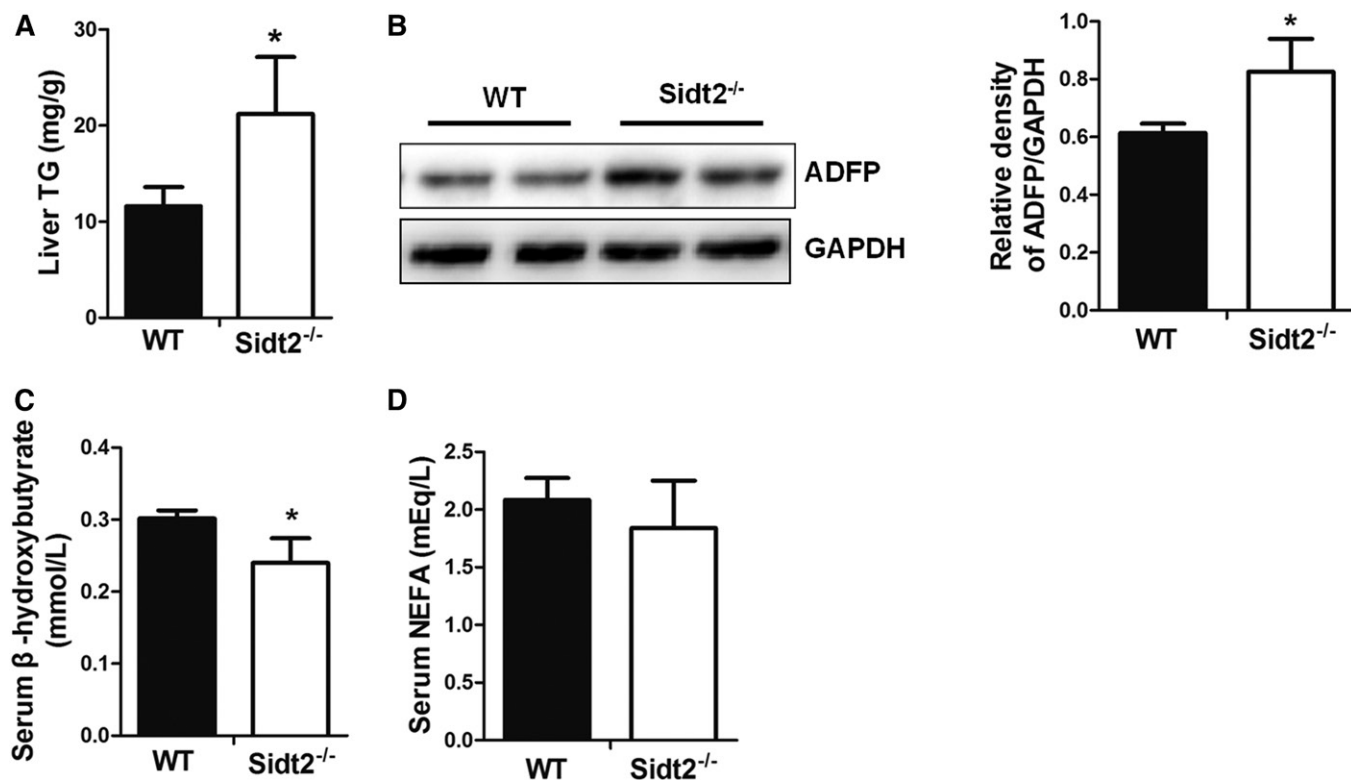


Fig. 3. *Sidt2* knockout reduces hepatic  $\beta$ -oxidation of fatty acids. A: Serum  $\beta$ -hydroxybutyrate levels of mice fed a chow diet (n = 6). B: Quantitative real-time PCR analysis of genes involved in lipolysis and fatty acid oxidation in livers of 14-week-old WT or *Sidt2*<sup>-/-</sup> mice fed a chow diet (n = 3). \*\**P* < 0.01.



**Fig. 4.** Lipid metabolism in 6-week-old mice fed with chow diet. **A:** Liver TG levels (n = 5). **B:** Immunoblot and densitometry analysis of ADFP levels in murine livers (n = 4). **C:** Serum  $\beta$ -hydroxybutyrate levels (n = 5). **D:** Serum NEFA levels of 6-week-old mice. (n = 5). \* $P < 0.05$ .

However, LC3-II levels in *Sidt2*<sup>-/-</sup> hepatocytes did not increase further in nutrient-free medium (Fig. 6B). Because either induction of autophagy or inhibition of autophagosome clearance could account for the increase in LC3-II levels, we measured autophagic flux by neutralizing lysosomal vacuolar pH with chloroquine. As shown in Fig. 6C, WT hepatocytes displayed a drastic increase in the levels of LC3-II in the presence of chloroquine (3.5-fold). By contrast, the response of *Sidt2*<sup>-/-</sup> hepatocytes was much less pronounced (1.3-fold), indicating that the autophagic flux had already been blocked by *Sidt2* deficiency.

The transmission EM also showed increased autophagic vacuoles at all stages of maturation in primary hepatocytes isolated from *Sidt2*<sup>-/-</sup> mice (Fig. 6E–I). And the number of autophagic vacuoles in *Sidt2*<sup>-/-</sup> hepatocytes was 3.3-fold of that in WT hepatocytes (Fig. 6J). These in vitro findings confirmed that *Sidt2* deficiency does not impair autophagosome formation, but interrupts the later stage.

#### Autophagy-related gene expression does not significantly change in livers of *Sidt2*<sup>-/-</sup> mice

Autophagosome formation is regulated at the molecular level by autophagy-related (Atg) genes. Among the corresponding Atg proteins, some are referred to as the “core” molecular machinery, as they are indispensable for autophagosome formation (31). In order to analyze whether *Sidt2* regulates the expression of Atg genes involved in core molecular machinery in vivo, we performed microarray analyses on *Sidt2*-deleted livers at 1, 3, and 6 months of age. In the liver transcriptome of *Sidt2*<sup>-/-</sup> mice,

*ULK1/2*, *Atg3*, *Atg5*, *Atg7*, *Atg12*, and *Beclin1* levels changed by less than  $\pm 2$ -fold, indicating that they were not significantly affected (Table 2), and these observations were in agreement with real-time PCR analysis (Fig. 7A). The levels of hepatic autophagy-related proteins (*Atg5*, *Atg7*, and *Beclin1*) in *Sidt2*<sup>-/-</sup> mice were also comparable to WT mice (Fig. 7B). These data suggest that *Sidt2* deficiency inhibits autophagy without changing RNA or protein expression of autophagy-related genes. Upregulation of LC3-II protein levels and increased autophagic vacuoles without enhanced autophagy initiation further confirmed that *Sidt2* deficiency leads to blockage during the terminal stage of autophagy.

In the course of autophagy, suppression of mTOR activity results in upregulation of lysosomal function (32). To address the status of mTOR kinase activity in *Sidt2*-depleted primary hepatocytes, we assessed levels of phosphorylation of S6K1 and 4E-BP1 by immunoblotting analysis. As shown in Fig. 7C, no significant difference was detected between endogenous phosphorylated S6K1 and 4E-BP1 in *Sidt2*-deficient hepatocytes compared with WT hepatocytes. Because mTORC1 is also a key upstream kinase that regulates the activity of TFEB (33), we assessed its protein expression by Western blot (Fig. 7D) and mRNA expression by GeneChip analysis (Table 2). The results showed that neither protein expression nor mRNA expression was changed in *Sidt2*<sup>-/-</sup> mice. Our data revealed that *Sidt2* deficiency does not significantly affect the mTOR signaling pathway.

As an integral LMP, *Sidt2* depletion could affect the structure and function of lysosomes. Therefore, we measured



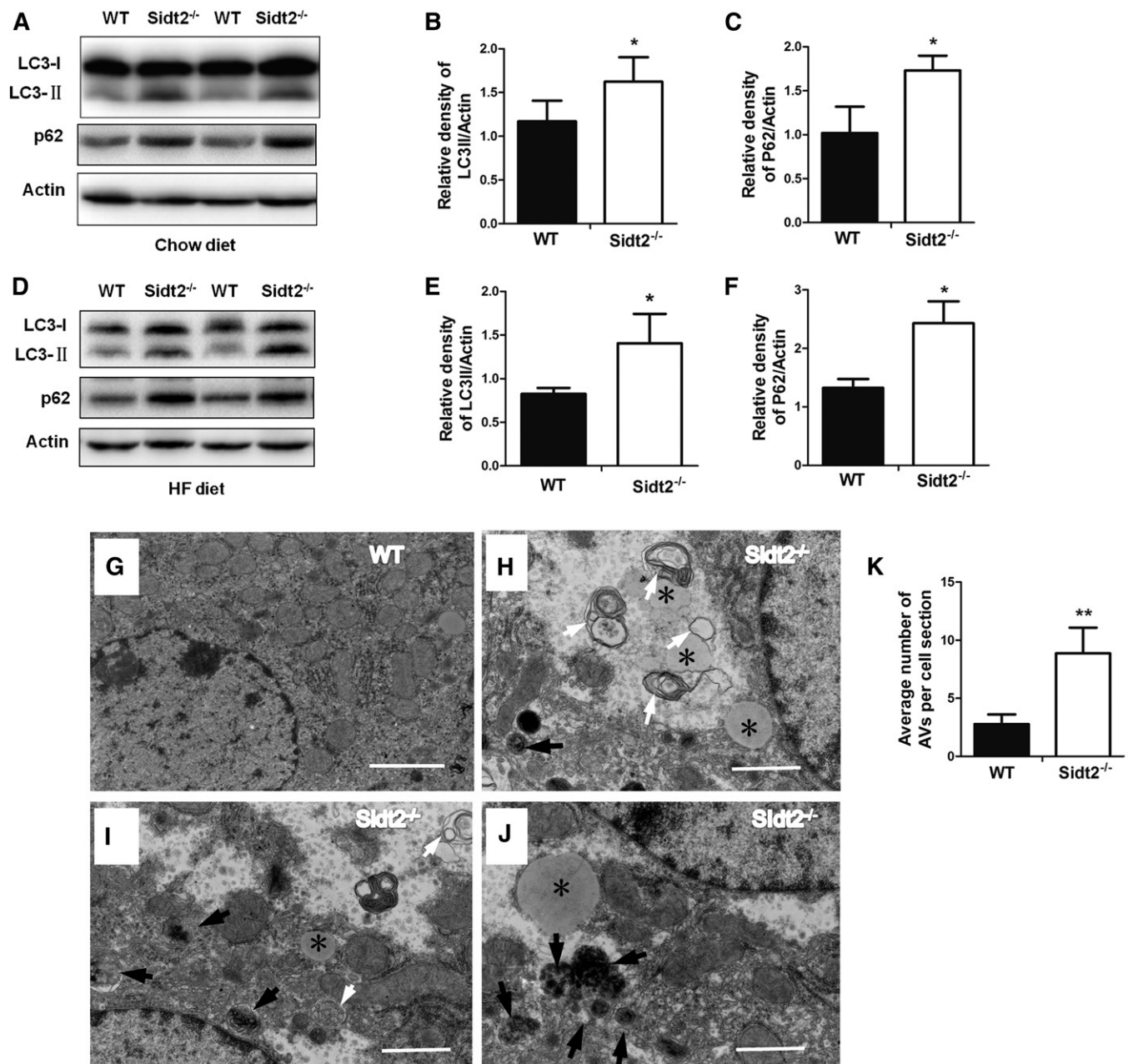


**Fig. 5.** *Sidt2* knockout blocks hepatic autophagy in vivo. A–C: Immunoblot analysis of LC3-II and p62 levels in livers from 14-week-old mice fed with chow diet ( $n = 4$ ). D–F: Immunoblot analysis of LC3-II and p62 levels in livers from mice fed with HF diet ( $n = 4$ ). EM of liver tissues from WT (G) and *Sidt2*<sup>-/-</sup> (H–J) mice. Abundant vacuolar structures were observed in *Sidt2*<sup>-/-</sup> livers. White arrows indicate autophagosomes and multi-lamellar membrane structures. Black arrows indicate autolysosomes. The asterisks indicate LDs. Scale bars: 2 μm (G); 1 μm (H–J). K: Quantification of autophagic vacuoles ( $n = 3$ ). \* $P < 0.05$ , \*\* $P < 0.01$ .

the protein expression levels of Lamp2 and lysosomal proteases, including cathepsin B and D. We detected that Lamp2 was increased in the livers of *Sidt2*<sup>-/-</sup> mice (Fig. 7E), which could be explained by accumulation of autolysosomes. As shown in Fig. 7F, the levels of mature cathepsin B in hepatic extracts of *Sidt2*<sup>-/-</sup> mice was lower (~1.5-fold) compared with the levels in WT mice. Pro-cathepsin B, as a precursor of cathepsin B, in hepatic extracts of *Sidt2*<sup>-/-</sup> mice was comparable to WT mice. Simultaneously, expression analysis of the *Ctsb* gene showed no significant difference between *Sidt2*<sup>-/-</sup> and WT mice. Cathepsin B is regulated at multiple levels, including transcription,

trafficking, and activation, so the results suggested that *Sidt2* deficiency could impair pro-cathepsin B transport or maturation in the lysosome, and consequently lead to reduced cathepsin B. We did not find significant differences in level of cathepsin D protein (mature form and immature form).

In addition, ASMase is a lysosomal enzyme expressed ubiquitously. Previous studies have revealed that changes in ASMase activity lead to autophagy dysregulation and contribute to the pathogenesis of fatty liver disease (28, 34); but we found no significant difference in ASMase activity between the two groups (Fig. 7G).



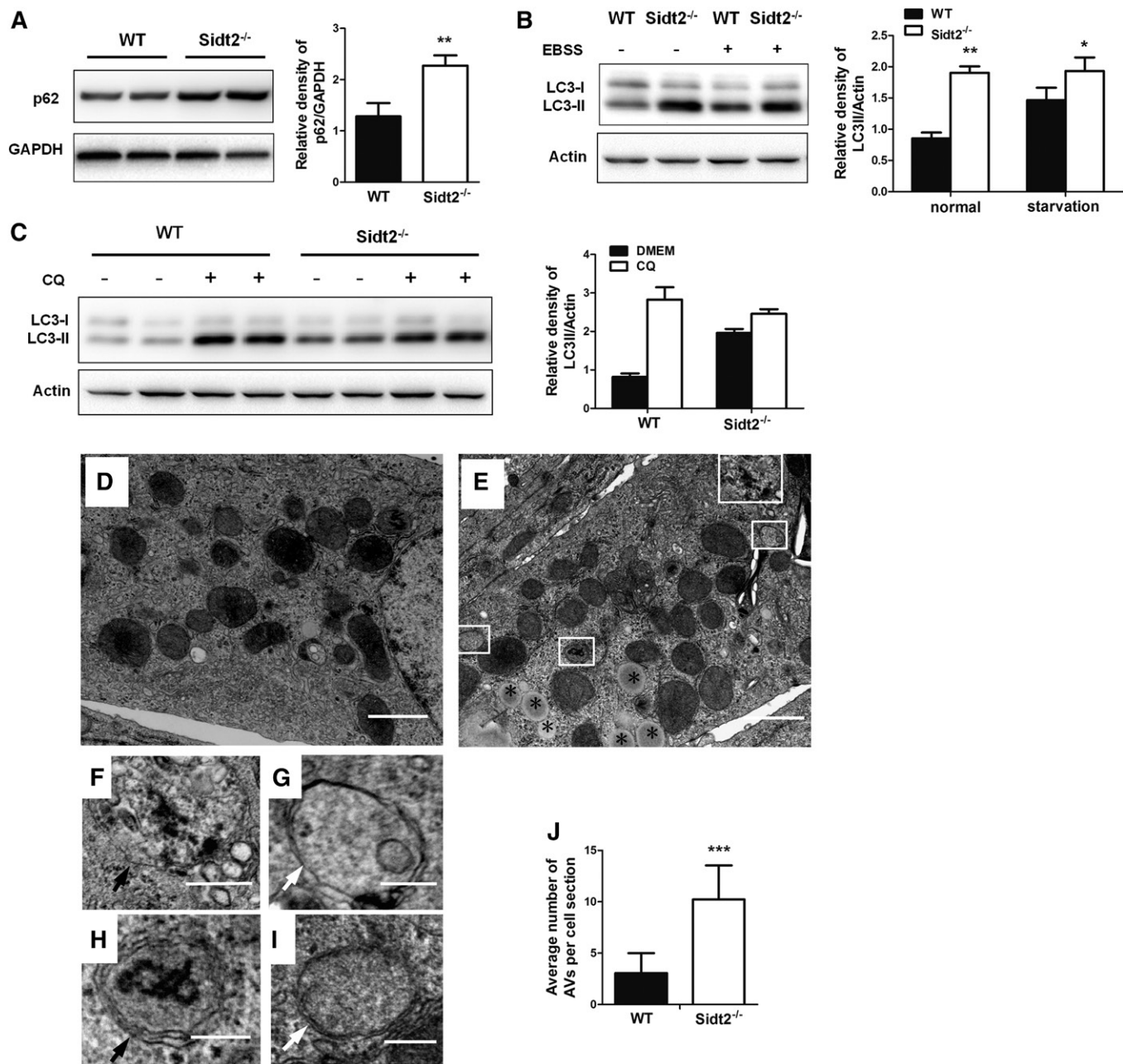


**Fig. 6.** *Sidt2* knockout blocks autophagy in vitro. **A:** Immunoblot analysis of p62 levels of primary hepatocytes from *Sidt2*<sup>-/-</sup> and WT mice in condition of normal medium. **B:** Immunoblot analysis of LC3-II levels in primary hepatocytes from *Sidt2*<sup>-/-</sup> and WT mice. Cells were either kept in normal medium or starved in Earle's balanced salt solution medium for 2 h. **C:** Primary hepatocytes were treated for 2 h with or without 30  $\mu$ M chloroquine, then the protein levels of LC3-II were detected by Western blot ( $n = 4$ ). **D–I:** Electron micrographs of primary hepatocytes cultured in normal medium from WT (**D**) and *Sidt2*<sup>-/-</sup> mice (**E–I**). **F–I:** Higher magnification images of the boxed area in **E** showing autophagosomes marked by white arrows and autolysosomes marked by black arrows. Scale bars: 1  $\mu$ m (**D**, **E**); 0.5  $\mu$ m (**F**); 0.2  $\mu$ m (**G–I**). **J:** Graph shows quantification of number of autophagic vacuoles (AVs) in hepatocytes ( $n = 14$  cells). \* $P < 0.05$ , \*\* $P < 0.01$ , and \*\*\* $P < 0.001$ . CQ, chloroquine.

## DISCUSSION

Integral LMPs are involved in various physiological processes, such as acidification of the lysosomal lumen and membrane fusion; thus, identification of more LMPs and further understanding their function has recently drawn more attention (9). In this study, mice with a global knockout of the *Sidt2* gene, an integral LMP, presented with increased liver volume and weight, accumulation of LDs,

and elevated hepatic TG levels. These characteristics resemble NAFLD in humans.

In contrast with the abundant content in adipose tissue, the liver has relatively low levels of cytosolic TG lipase and Hsl (35). Thus, the liver needs an additional pathway to digest fat. Autophagy is a critical pathway contributing to the liver's rapid turnover of TG (12). Portions of LDs, or even whole droplets, become sequestered inside the double membrane-bound vesicles and

TABLE 2. The mRNA expression of autophagy-related genes in *Sidt2*<sup>-/-</sup> relative to WT mice

Gene Symbol	Gene Title	Fold Change (KO/WT)		
		1 Month	3 Months	6 Months
<i>Ulk1</i>	Unc-51 like kinase 1	-1.25	1.10	-1.44
<i>Ulk2</i>	Unc-51 like kinase 2	-1.04	1.24	-1.34
<i>Atg13</i>	ATG13 autophagy related 13 homolog	-1.04	1.02	-1.01
<i>Map1lc3b</i>	Microtubule-associated protein 1 light chain 3β	-1.05	-1.09	1.22
<i>Atg5</i>	Autophagy related 5	1.41	1.19	0.85
<i>Atg12</i>	Autophagy related 12	1.20	1.06	0.92
<i>Atg3</i>	Autophagy related 3	1.15	1.24	-1.47
<i>Atg7</i>	Autophagy related 7	-1.13	-1.13	-1.35
<i>Beclin1</i>	Beclin 1, autophagy related	1.19	1.31	-1.08
<i>Atg14</i>	Autophagy related 14	-1.12	-1.39	-1.10
<i>Uvrag</i>	UV radiation resistance associated gene	-1.05	-1.06	-1.22
<i>Atg9a</i>	Autophagy-related 9A	-1.13	-1.08	1.01
<i>Atg9b</i>	ATG9 autophagy related 9 homolog B	1.23	1.02	1.09
<i>Atg10</i>	Autophagy related 10	1.08	1.49	-1.05
<i>Tcf7l1</i>	Transcription factor EB	-1.09	1.03	1.31

are delivered to lysosomes, where they are degraded to fatty acids. The autophagy-related lipid degradation pathway allows hepatocytes to rapidly mobilize large amounts of lipids despite their lower levels of cytosolic lipases compared with adipose tissues (36). When pharmacologic or genetic factors inhibit autophagy in hepatocytes, breakdown of stored lipids to supply fatty acids for β-oxidation is blocked (12).

First, enhanced lipogenesis, reduced TG secretion, diminished liver lipolysis, and excess lipolysis in adipose tissue were excluded as a possible cause of TG accumulation in the *Sidt2*<sup>-/-</sup> liver. Second, several lines of investigation demonstrated that defective autophagy may contribute to the TG accumulation in *Sidt2*-deficient mice, including elevated p62 and LC3-II, EM evidence of autophagosome accumulation in the liver, and decreased serum levels of β-hydroxybutyrate.

The terminal stage of autophagy involves the fusion of autophagosomes with endosomes/lysosomes and sequential substrate degradation (37). Our in vitro analysis showed that, in primary hepatocytes isolated from *Sidt2*<sup>-/-</sup> mice, the high levels of LC3-II detected in basal conditions were not further increased by chloroquine treatment. This observation revealed that *Sidt2* deficiency impaired autophagy at the terminal stage rather than the initial stage of autophagosome formation. This hypothesis was supported by unchanged mRNA expression of autophagy-related genes involved in autophagy initiation. EM analysis of both in vivo and in vitro experiments showed that *Sidt2* deficiency caused accumulation of autophagosomes. Thus, we inferred that maturation of autophagosomes was blocked in *Sidt2*<sup>-/-</sup> mice.


Cathepsin B is synthesized in the rough endoplasmic reticulum as a proenzyme and then it turns into pro-cathepsin B after removing the signal peptide. Pro-cathepsin B is glycosylated in the Golgi apparatus and is transported to lysosomes where it is proteolytically cleaved to form a mature protein. A reduced level of mature cathepsin B and an unchanged level of pro-cathepsin B in *Sidt2*<sup>-/-</sup> liver, along with normal mRNA for *Ctsb*, implied that *Sidt2* could affect pro-cathepsin B transport or maturation in

the lysosomes. It has been reported that reduction of cathepsin B and D contributes to dysfunctional autophagy by delayed degradation of autolysosomes and defective lysosome reformation (38). The role of decreased mature cathepsin B in *Sidt2*<sup>-/-</sup> liver should be further investigated. We found no significantly reduced level of another major lysosomal protease, cathepsin D, underscoring the high sensitivity of cathepsin B to variation of lysosome homeostasis.

The impact of *Sidt2* on autophagy is reminiscent of LAMP-2, one of the most abundant LMPs. LAMP-2 deficiency causes Danon disease in humans and a similar phenotype in mouse models. Previously, autophagosome accumulation in LAMP-2-deficient mice was shown to be secondary to slow maturation of the autophagosomes rather than increased formation (39, 40). Further study is necessary to investigate whether there is interaction between *Sidt2* and LAMP-2.

Our previous studies revealed that a global *Sidt2* gene knockout mouse exhibited age-dependent elevated plasma glucose levels and impaired glucose tolerance at 8 weeks of age (41). However, *Sidt2*<sup>-/-</sup> mice at 6 weeks of age already displayed elevated liver TG content and decreased serum β-hydroxybutyrate level, which minimized the effect of hyperglycemia on lipid metabolism to some extent. To address the direct effects of *Sidt2* on the liver, future studies in liver-specific *Sidt2* knockout models should be performed.

In our study, the mice fed a HF diet exhibited a much more pronounced phenotype in fatty infiltration of the liver compared with mice fed a chow diet. *Sidt2*<sup>-/-</sup> mice fed a HF diet even showed manifestation of steatohepatitis, such as ballooning degeneration. This finding suggests that *Sidt2* may play an important role in accommodating a chronic exogenous lipid challenge.

In summary, our study demonstrates that *Sidt2* is critical in mouse TG catabolism by regulating autophagy at its terminal stage. Therefore, *Sidt2* may be a target of therapeutic intervention of NAFLD. 

The authors thank Prof. Zhang Zhiguo and Prof. Yang Jian of the Department of Endocrinology, Ruijin Hospital, Shanghai

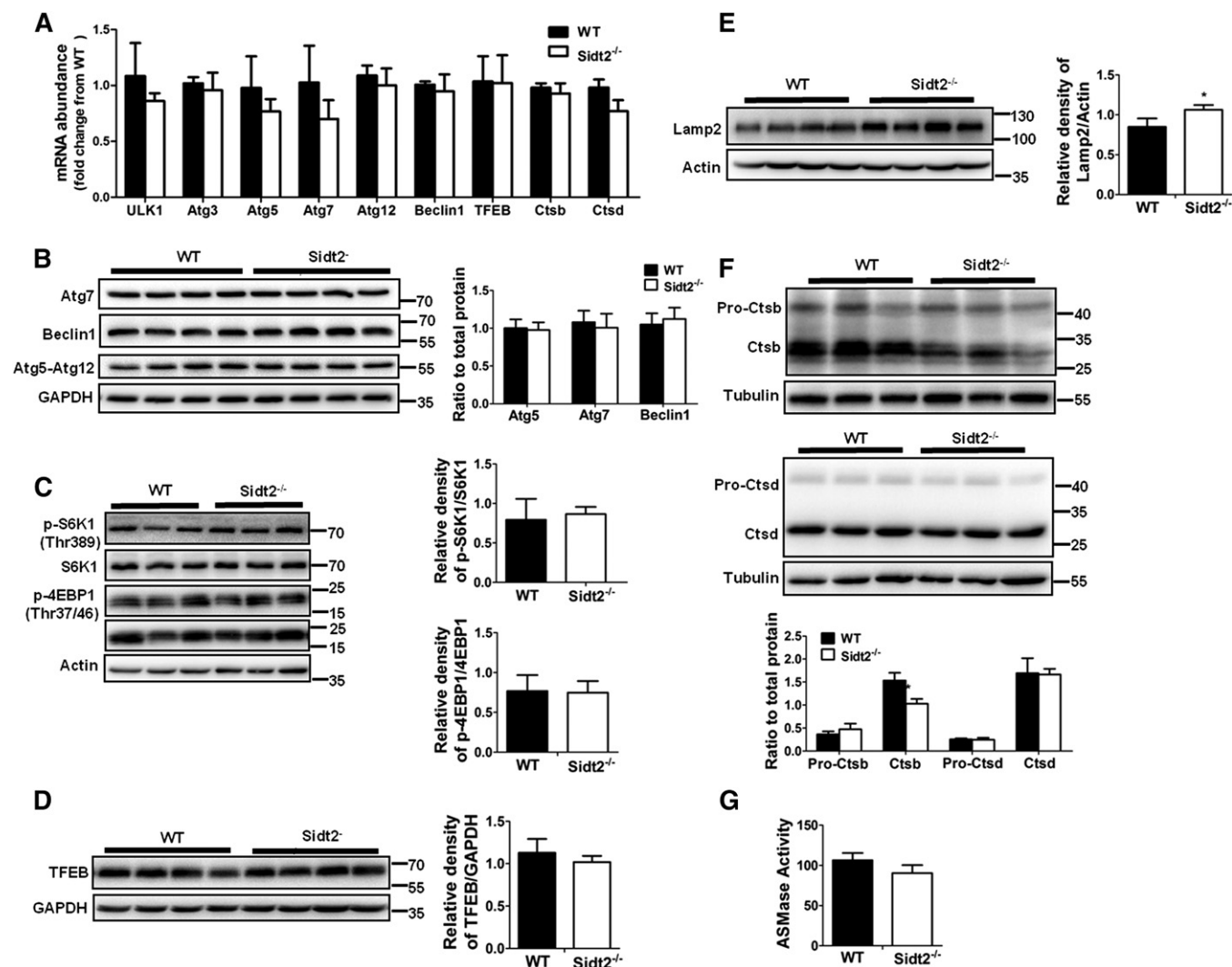


**Fig. 7.** Autophagy-related gene expression does not significantly change in livers of *Sidt2*<sup>-/-</sup> mice. **A:** Quantitative real-time PCR analysis of genes involved in autophagy and lysosomal proteases in livers of 14-week-old WT or *Sidt2*<sup>-/-</sup> mice fed a chow diet (n = 3). **B:** Immunoblot analysis of Beclin1, Atg5, and Atg7 levels in livers from 14-week-old mice fed with chow diet (n = 4). **C:** Phospho-S6K1, S6K1, phospho-4E-BP1, and 4E-BP1 of primary hepatocytes in RM from *Sidt2*<sup>-/-</sup> and WT mice (n = 4). **D–F:** Immunoblot analysis of TFEB (D), Lamp2 (E), cathepsin B and cathepsin D (in their immature and mature forms) (F) in mouse livers. **G:** ASMase activity in liver lysates from *Sidt2*<sup>-/-</sup> and WT mice fed a chow diet (n = 3–4). \*P < 0.05. Ctsb, cathepsin B; Ctsd, cathepsin D.

Jiao Tong University for their generous assistance with primary hepatocyte culture.

## REFERENCES

- Saftig, P., and J. Klumperman. 2009. Lysosome biogenesis and lysosomal membrane proteins: trafficking meets function. *Nat. Rev. Mol. Cell Biol.* **10**: 623–635.
- Conus, S., and H. U. Simon. 2008. Cathepsins: key modulators of cell death and inflammatory responses. *Biochem. Pharmacol.* **76**: 1374–1382.
- Divangahi, M., M. Chen, H. Gan, D. Desjardins, T. T. Hickman, D. M. Lee, S. Fortune, S. M. Behar, and H. G. Remold. 2009. Mycobacterium tuberculosis evades macrophage defenses by inhibiting plasma membrane repair. *Nat. Immunol.* **10**: 899–906.
- Coxon, F. P., and A. Taylor. 2008. Vesicular trafficking in osteoclasts. *Semin. Cell Dev. Biol.* **19**: 424–433.
- Boustany, R. M. 2013. Lysosomal storage diseases—the horizon expands. *Nat. Rev. Neurol.* **9**: 583–598.
- Kirkegaard, T., and M. Jaattela. 2009. Lysosomal involvement in cell death and cancer. *Biochim. Biophys. Acta.* **1793**: 746–754.
- Nixon, R. A., D. S. Yang, and J. H. Lee. 2008. Neurodegenerative lysosomal disorders: a continuum from development to late age. *Autophagy.* **4**: 590–599.
- Lutgens, S. P., K. B. Cleutjens, M. J. Daemen, and S. Heeneman. 2007. Cathepsin cysteine proteases in cardiovascular disease. *FASEB J.* **21**: 3029–3041.
- Settembre, C., and A. Ballabio. 2014. Lysosome: regulator of lipid degradation pathways. *Trends Cell Biol.* **24**: 743–750.
- Koo, S. H. 2013. Nonalcoholic fatty liver disease: molecular mechanisms for the hepatic steatosis. *Clin. Mol. Hepatol.* **19**: 210–215.
- Postic, C., and J. Girard. 2008. Contribution of de novo fatty acid synthesis to hepatic steatosis and insulin resistance: lessons from genetically engineered mice. *J. Clin. Invest.* **118**: 829–838.
- Singh, R., S. Kaushik, Y. Wang, Y. Xiang, I. Novak, M. Komatsu, K. Tanaka, A. M. Cuervo, and M. J. Czaja. 2009. Autophagy regulates lipid metabolism. *Nature.* **458**: 1131–1135.
- Schwake, M., B. Schroder, and P. Saftig. 2013. Lysosomal membrane proteins and their central role in physiology. *Traffic.* **14**: 739–748.
- Saftig, P., B. Schroder, and J. Blanz. 2010. Lysosomal membrane proteins: life between acid and neutral conditions. *Biochem. Soc. Trans.* **38**: 1420–1423.



15. Schröder, B. A., C. Wrocklage, A. Hasilik, and P. Saftig. 2010. The proteome of lysosomes. *Proteomics*. **10**: 4053–4076.
16. Eskelinen, E. L., Y. Tanaka, and P. Saftig. 2003. At the acidic edge: emerging functions for lysosomal membrane proteins. *Trends Cell Biol.* **13**: 137–145.
17. Chapel, A., S. Kieffer-Jaquinod, C. Sagne, Q. Verdon, C. Ivaldi, M. Mellal, J. Thirion, M. Jadot, C. Bruley, J. Garin, et al. 2013. An extended proteome map of the lysosomal membrane reveals novel potential transporters. *Mol. Cell. Proteomics*. **12**: 1572–1588.
18. Callahan, J. W., R. D. Bagshaw, and D. J. Mahuran. 2009. The integral membrane of lysosomes: its proteins and their roles in disease. *J. Proteomics*. **72**: 23–33.
19. Jialin, G., G. Xuefan, and Z. Huiwen. 2010. SID1 transmembrane family, member 2 (Sidt2): a novel lysosomal membrane protein. *Biochem. Biophys. Res. Commun.* **402**: 588–594.
20. Chang, G., R. Yang, Y. Cao, A. Nie, X. Gu, and H. Zhang. 2016. SIDT2 is involved in the NAADP-mediated release of calcium from insulin secretory granules. *J. Mol. Endocrinol.* **56**: 249–259.
21. Gao, J., X. Gu, D. J. Mahuran, Z. Wang, and H. Zhang. 2013. Impaired glucose tolerance in a mouse model of sidt2 deficiency. *PLoS One*. **8**: e66139.
22. Tanaka, M., and A. Miyajima. 2012. Identification and isolation of adult liver stem/progenitor cells. *Methods Mol. Biol.* **826**: 25–32.
23. Choi, S. E., S. M. Lee, Y. J. Lee, L. J. Li, S. J. Lee, J. H. Lee, Y. Kim, H. S. Jun, K. W. Lee, and Y. Kang. 2009. Protective role of autophagy in palmitate-induced INS-1 beta-cell death. *Endocrinology*. **150**: 126–134.
24. Teufel, A., T. Maass, S. Strand, S. Kanzler, T. Galante, K. Becker, D. Strand, S. Biesterfeld, H. Westphal, and P. R. Galle. 2010. Liver-specific Ldb1 deletion results in enhanced liver cancer development. *J. Hepatol.* **53**: 1078–1084.
25. Millar, J. S., D. A. Cromley, M. G. McCoy, D. J. Rader, and J. T. Billheimer. 2005. Determining hepatic triglyceride production in mice: comparison of poloxamer 407 with Triton WR-1339. *J. Lipid Res.* **46**: 2023–2028.
26. Norris, A. W., L. Chen, S. J. Fisher, I. Szanto, M. Ristow, A. C. Jozsi, M. F. Hirshman, E. D. Rosen, L. J. Goodyear, F. J. Gonzalez, et al. 2003. Muscle-specific PPARgamma-deficient mice develop increased adiposity and insulin resistance but respond to thiazolidinediones. *J. Clin. Invest.* **112**: 608–618.
27. Hajri, T., X. X. Han, A. Bonen, and N. A. Abumrad. 2002. Defective fatty acid uptake modulates insulin responsiveness and metabolic responses to diet in CD36-null mice. *J. Clin. Invest.* **109**: 1381–1389.
28. Ferré, P., and F. Foufelle. 2010. Hepatic steatosis: a role for de novo lipogenesis and the transcription factor SREBP-1c. *Diabetes Obes. Metab.* **12**(Suppl 2): 83–92.
29. Kimura, S., N. Fujita, T. Noda, and T. Yoshimori. 2009. Monitoring autophagy in mammalian cultured cells through the dynamics of LC3. *Methods Enzymol.* **452**: 1–12.
30. Kawano, Y., and D. E. Cohen. 2013. Mechanisms of hepatic triglyceride accumulation in non-alcoholic fatty liver disease. *J. Gastroenterol.* **48**: 434–441.
31. Xie, Z., and D. J. Klionsky. 2007. Autophagosome formation: core machinery and adaptations. *Nat. Cell Biol.* **9**: 1102–1109.
32. Zhou, J., S. H. Tan, V. Nicolas, C. Bauvy, N. D. Yang, J. Zhang, Y. Xue, P. Codogno, and H. M. Shen. 2013. Activation of lysosomal function in the course of autophagy via mTORC1 suppression and autophagosome-lysosome fusion. *Cell Res.* **23**: 508–523.
33. Martina, J. A., Y. Chen, M. Gucek, and R. Puertollano. 2012. mTORC1 functions as a transcriptional regulator of autophagy by preventing nuclear transport of TFEB. *Autophagy*. **8**: 903–914.
34. Garcia-Ruiz, C., J. M. Mato, D. Vance, N. Kaplowitz, and J. C. Fernandez-Checa. 2015. Acid sphingomyelinase-ceramide system in steatohepatitis: a novel target regulating multiple pathways. *J. Hepatol.* **62**: 219–233.
35. Christian, P., J. Sacco, and K. Adeli. 2013. Autophagy: emerging roles in lipid homeostasis and metabolic control. *Biochim. Biophys. Acta.* **1831**: 819–824.
36. Zechner, R., and F. Madeo. 2009. Cell biology: another way to get rid of fat. *Nature*. **458**: 1118–1119.
37. Shen, H. M., and N. Mizushima. 2014. At the end of the autophagic road: an emerging understanding of lysosomal functions in autophagy. *Trends Biochem. Sci.* **39**: 61–71.
38. Tatti, M., M. Motta, S. Di Bartolomeo, V. Cianfanelli, and R. Salvioli. 2013. Cathepsin-mediated regulation of autophagy in saposin C deficiency. *Autophagy*. **9**: 241–243.
39. González-Polo, R. A., P. Boya, A. L. Pauleau, A. Jalil, N. Larochette, S. Souquère, E. L. Eskelinen, G. Pierron, P. Saftig, and G. Kroemer. 2005. The apoptosis/autophagy paradox: autophagic vacuolization before apoptotic death. *J. Cell Sci.* **118**: 3091–3102.
40. Tanaka, Y., G. Guhde, A. Suter, E. L. Eskelinen, D. Hartmann, R. Lullmann-Rauch, P. M. Janssen, J. Blanz, K. von Figura, and P. Saftig. 2000. Accumulation of autophagic vacuoles and cardiomyopathy in LAMP-2-deficient mice. *Nature*. **406**: 902–906.
41. Mao, H., W. Gao, C. Ma, J. Sun, J. Liu, Q. Shao, B. Song, and X. Qu. 2013. Human placental trophoblasts express the immunosuppressive cytokine IL-35. *Hum. Immunol.* **74**: 872–877.